Electromagnetic Non-Destructive Evaluation (XXI)
D. Lesselier and C. Reboud (Eds.)

doi:10.3233/978-1-61499-836-5-175

Fast Models Dedicated to Simulation of Eddy Current Thermography

Almpion RATSAKOU [a,1], Christophe REBOUD [a], Anastasios SKARLATOS [a] and Dominique LESSELIER [b]

[a] *CEA, LIST, Centre de Saclay, Gif-sur-Yvette F-91191, France*
[b] *Laboratoire des Signaux et Systèmes (UMR8506, CNRS-CentraleSupélec-Univ. Paris Sud), Université Paris-Saclay, 91192 Gif-sur-Yvette cedex, France*

Abstract. This communication presents the first development aiming at efficiently simulating configurations of eddy current thermography for nondestructive evaluation. The numerical method proposed here is based on the Finite Integration Technique for both electromagnetic and thermal problems. Simulation results obtained using two different materials, steel and aluminum, are compared and discussed with respect to the presence of a flaw affecting the piece under test.

Keywords. Eddy current, thermography, simulation, finite integration technique

1. Introduction

The use of thermography [1] for nondestructive testing applications had received growing attention in the last years. This is mainly due to the fact that infrared (IR) cameras have recently improved significantly in both sensitivity and spatial resolution and that this technique is particularly adapted to many applications [2] such as composites' inspection. Unlike other direct imaging techniques, it is a fast, high resolution and contactless method. Thermal testing is generally divided into two main streams: passive and active. Passive thermography is defined as measuring the temperature difference between the target material and its surroundings under different ambient temperature conditions. Active thermography uses a thermal source in order to deposit heat in the target material. Most common sources consist in lamps or lasers [3] that heat part of the piece surface. These techniques of depositing heat on the materials have potential disadvantages, *e.g.* the reflected heat from the material can interfere with the measured signals, causing signal-to-noise-ratio (SNR) problems. For instance, many conductive materials when used in industry are coated or painted. The heating of the workpiece may also be obtained via the application of sonic or ultrasonic energy using a welding horn, *i.e.* vibrothermography, thermosonics or sonic infrared [4]. In this case, however, contact between the workpiece and the ultrasonic welding horn it is required, which can complicate its practical use and cause a loss of energy transmission.

[1] Corresponding Author: Almpion Ratsakou, CEA, LIST, Centre de Saclay, Gif-sur-Yvette F-91191, France; E-mail:almpion.ratsakou@cea.fr.

Eddy current thermography (ECT), also named as induction thermography, is an alternative to inspect metallic structures that does not suffer from the above-mentioned disadvantages. This is an emerging technology in nondestructive testing (NdT) that combines eddy current and thermography. ECT is based on electromagnetic induction and Joule effect heating. The technique uses induced eddy current to heat the sample and defect detection is based on the changes of the induced eddy current flow revealed by the thermal visualization captured by an IR camera. Induction thermography can be used to detect cracks [5], disbond, impact damage, delamination and corrosion.

This work presents a modelling approach using a two-dimensional numerical solver based on the Finite Integration Technique (FIT) [6,7]. A typical configuration, consisting of a coil located above a plate, is sketched in Figure 1. This configuration will be used in our simulations and an axial symmetry is assumed. The same numerical tool is used to solve both physical problems, namely the electromagnetic induction by the coil in the plate and the heat diffusion in the plate after excitation. Due to the large difference in time scale between the electromagnetic problem and the thermal one, a weak coupling of the two problems is possible.

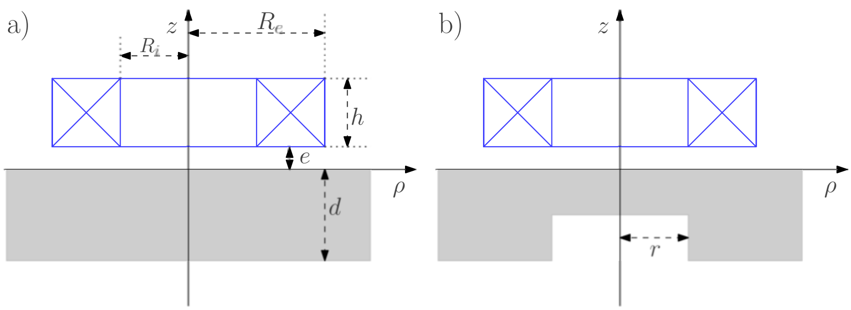

Figure 1. Schematic setup diagram. Circular coil of inner radius R_i, outer radius R_e and height h standing above a conductive plate of thickness d in a distance e. **a)** Homogeneous plate. **b)** Homogeneous plate with a axisymmetric defect of radius r.

In other words, the electromagnetic problem is first solved to calculate the time-dependent eddy current density induced in the plate, then it is converted into a heat source term by considering Joule effect. Finally, the diffusion of heat in the plate is computed with respect to time. This first development will serve as reference for further works, consisting in solving both problems with fast modal methods [8].

2. Theoretical formulation

ECT involves multi-physical interactions with electromagnetic-thermal phenomena including eddy current, Joule heating and heat conduction. Simulation of induction heating requires the ability to model multiple physical fields. Thus, modeling the generation of eddy current requires an electromagnetic solution in the workpiece, which results in a Joule heat distribution. The latter is used as a volumetric heating source in order to obtain the temperature distribution in the workpiece.

The coupling between the electromagnetic problem and the thermal one can often be further complicated by the fact that the electromagnetic properties of the workpiece are depending on the temperature of the workpiece, which will lead to a strongly-coupled problem. This coupling of the two problems requires the electromagnetic solution to be computed based on a time/temperature updated set of materials properties. This leads to a time consuming numerical computation that can be avoided under some assumptions.

The induction heating process involves multiple time and length scales. Generally, the time scale associated with the heat transfer is much larger than the time scale associated with the electromagnetics. The time scale associated with the electromagnetic solution depends on the frequency f of the alternative current in the coil, while the time scale associated with the transient heat transfer in the workpiece is determined by its thermal properties. The length scale, for the electromagnetic problem, also depends on the frequency, as well on the magnetic permeability μ and electrical conductivity σ. The so-called *skin depth*, defined in the particular case of a half-space medium by the relation $\delta = (\pi\mu\sigma f)^{-1/2}$, illustrates the penetration of the electromagnetic field in the piece. As a consequence, the associated Joule effect is also generated in a depth range of two or three times the skin depth δ. From the numerical point of view, this implies that this particular region must be finely discretized.

2.1. The electromagnetic problem

In a typical configuration, a pulse generator emits a signal to an infrared camera and to a induction heater, which generates an excitation signal. This excitation signal is usually a sinusoidal of alternating current with high amplitude. The current is then driven into an inductive coil, which induces eddy current in the neighbouring workpiece. This phenomenon is described by the Maxwell's equations, which for the quasi-static approximation are

$$\nabla \times \mathbf{E} = -\frac{\partial \mathbf{B}}{\partial t}, \tag{1}$$

$$\nabla \times \mathbf{H} = \mathbf{J}, \tag{2}$$

$$\nabla \cdot \mathbf{B} = 0, \tag{3}$$

where $\mathbf{E}$ is the electric field intensity, $\mathbf{H}$ is the magnetic field intensity, $\mathbf{B}$ is the magnetic flux density, and $\mathbf{J}$ is the current density. Excitation frequencies are typically lower than 10 MHz, consequently the displacement current term $(\partial\mathbf{D}/\partial t)$ in (2) can be neglected. The above equations are combined with the following constitutive relations characterizing a linear, homogeneous and isotropic material

$$\mathbf{J} = \sigma\mathbf{E}, \qquad \mathbf{B} = \mu\mathbf{H}. \tag{4}$$

For solving the above differential equations and since $\mathbf{B}$ is divergence free, it can be expressed as $\mathbf{B} = \nabla \times \mathbf{A}$ where $\mathbf{A}$ is the magnetic vector potential. Substituting $\mathbf{B}$ into (1) and using (2) as well as the constitutive relations (4), the diffusion equation for the magnetic vector potential can be derived as:

$$\nabla \times \mu^{-1}\nabla \times \mathbf{A} + \sigma\frac{\partial \mathbf{A}}{\partial t} = \mathbf{J}_s \tag{5}$$

where $\mathbf{J}_s$ is the current density driving the inductor. The choice of a Coulomb gauge, $\nabla \cdot \mathbf{A} = 0$, is made here.

The FIT method provides a discrete reformulation of Maxwell's equations on its integral form. A typical simulation task is described by a known geometry and material configuration, as well as boundary and initial conditions. In the following a rectangular cubic cell complex consisting of a material grid complex $\mathbf{M}$, a primary grid complex $\mathbf{G}$ and a dual grid complex $\widetilde{\mathbf{G}}$ will be used.

The eddy current density in FIT is computed by the equation

$$\widetilde{\mathbf{C}}\mathbf{M}_{\mu}^{-1}\mathbf{C}\widehat{\mathbf{a}} - \mathbf{M}_{\sigma}\dot{\widehat{\mathbf{a}}} = \widehat{\widehat{\mathbf{j}}} \tag{6}$$

where $\widetilde{\mathbf{C}}$ and $\mathbf{C}$, contain only topological information and represent a discrete curl-operator on the primary and the dual grid $\mathbf{G}$ and $\widetilde{\mathbf{G}}$, respectively, $\mathbf{M}_{\mu}^{-1}$, $\mathbf{M}_{\sigma}$, are the material matrices, $\widehat{\mathbf{a}}$ is the magnetic vector potential and $\widehat{\widehat{\mathbf{j}}}$ is the current density.

Initial conditions of the model assume a thermal equilibrium of the sample and its surroundings. In the z-direction Neumann boundary conditions are imposed. On the artificial left side boundary, at $\rho = 0$ where the axis of the symmetry is, Neumann condition is imposed too. On the right side boundary, at $\rho = \rho_e$ Dirichlet boundary condition is imposed. We suppose that the workpiece is infinite in the ρ-direction so this artificial boundary does not affect the solution within the domain of interest.

2.2. The thermal problem

Due to resistive heating from the induced eddy current, the temperature of conductive materials increases, which is known as Joule heating. It can be expressed by the equation

$$\dot{Q} = \frac{1}{\sigma}\,|\mathbf{J_s}|^2\,,$$

where the sum of generated power density $\dot{Q}$ is proportional to the square of the eddy current density. The resistive heat will diffuse as a time transient until an equilibrium state is restored between the bulk and its surface, or better saying the workpiece and the environment. The thermal part of the problem can be divided into two phases, *(i)* the heating phase, during which the heat is being deposited in the workpiece and *(ii)* the cooling phase, when the workpiece has reached a maximum temperature, the deposit of heat has stopped, and only diffusion of the heat is occurring in the plate.

Starting with the energy conservation law in integral form

$$\int_V \varrho\, C_p \frac{\partial T}{\partial t}\,\mathrm{d}V = \int_V \dot{Q}\,\mathrm{d}V - \oint_{\partial V} \mathbf{J} \cdot \mathrm{d}\mathbf{s} \tag{7}$$

and using the Fourier's law $\mathbf{J} = -\kappa \nabla T$, the heat equation is derived as

$$-\kappa \nabla^2 T + \varrho\, C_p \frac{\partial T}{\partial t} = \dot{Q}, \tag{8}$$

where κ is the thermal conductivity, ϱ the density, C_p the specific heat and T the temperature.

In the FIT, the solution of the thermal problem is given by the equation

$$\widetilde{\mathbf{S}}\mathbf{M}_{\kappa}\mathbf{G}\theta - \mathbf{M}_{c}\dot{\theta} = -\dot{\mathbf{q}}, \tag{9}$$

which is a discrete formulation for the heat equation, where $\widetilde{\mathbf{S}}$ is the div-operator on the dual grid, $\mathbf{M}_{\kappa}$, $\mathbf{M}_{c}$ are material matrices, $\mathbf{G}$ is the discrete gradient matrix, θ the temperature and $\dot{\mathbf{q}}$ the source term.

Pairing this equation with the boundary conditions, the temperature of the workpiece and its surrounding is computed. The boundary conditions that are used here are the same as in the electromagnetic problem.

3. Simulation and results

For the simulations a circular coil is used with $e = 1$ mm of lift-off and inner radius $R_i = 11$ mm, outer radius $R_e = 84$ mm, height $h = 41$ mm and number of wire-turns $N = 408$ as in [9]. For modeling the workpiece, two different materials are used: (i) Aluminum, (ii) Steel, their respective physical parameters being given in Table 1. We are investigating here two scenarios. In the first case, we compare the behaviours of two homogeneous plates of thickness $d = 10$ mm, made of aluminum and steel, respectively. In the second case, we introduce a defect, which can be assumed to be a corrosion, at the bottom surface of a thin plate ($d = 1$ mm) of aluminum. The defect is modelled as a local change of physical properties (same as the surrounding environment). The excitation signal is considered to be a sinusoid of frequency f. Setting the frequency of the excitation signal at $f = 200$ Hz and the duration of the signal at 50 ms we probe the two different plates with 10 periods of the signal. In Figure 2, the images of the simulation for three crucial times are given. In the first two rows, for which no diffusion has been occurring, the skin depth effect is highlighted, i.e. the difference of the electromagnetic properties of the materials.

As one can expect, through the Joule effect, the penetration depth of the eddy currents in the aluminum plate is much larger than in the workpiece of steel. The difference between both rows of images is a result of the difference of the thermal properties of the materials. A corrosion has been now introduced in a thick aluminum plate. The frequency of the probed signal has been kept the same, at 200 Hz, which gives a penetration depth of 6 mm, much larger than the thickness of the plate. The defect has been modeled as a circular discontinuity in the plane (ρ, θ) of radius $r = 3$ cm or 5 cm and a thickness of 0.5 mm in the z-direction. The results of the simulation of this setup are given in Figure 3.

Since only the infrared radiation emitted by the surface of the workpiece as a function of time can be captured by a thermal camera, in Figure 4 and Figure 5 the surface temperatures are plotted. In Figure 4, the temperature of the the workpiece on the sur-

Table 1. Electromagnetic and thermal parameters of the materials.

	μ_r	σ (S/m)	κ (W/m/K)	ϱ (Kg/m^3)	C_p (J/Kg/K)
Aluminum case	1	3.5×10^7	237	2707	897
Steel	700	3.21×10^6	44.5	7850	475

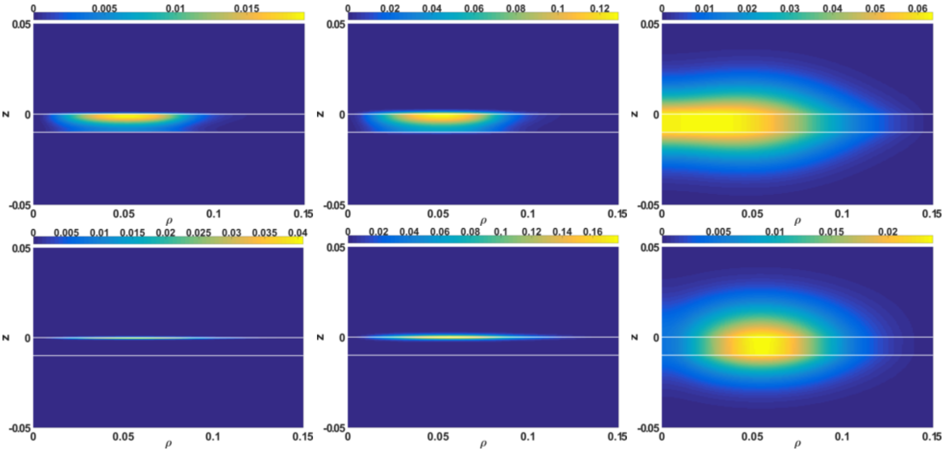

Figure 2. Temperature distribution images in the region of interest for different time and homogeneous materials without defects.
Top: Aluminum. *Left to the right:* Different observation times, $t = t_0$, $t = t_0 + 50$ ms, $t = t_0 + 5$s.
Bottom: Steel. *Left to the right:* Different observation times, $t = t_0$, $t = t_0 + 50$ ms, $t = t_0 + 5$s.

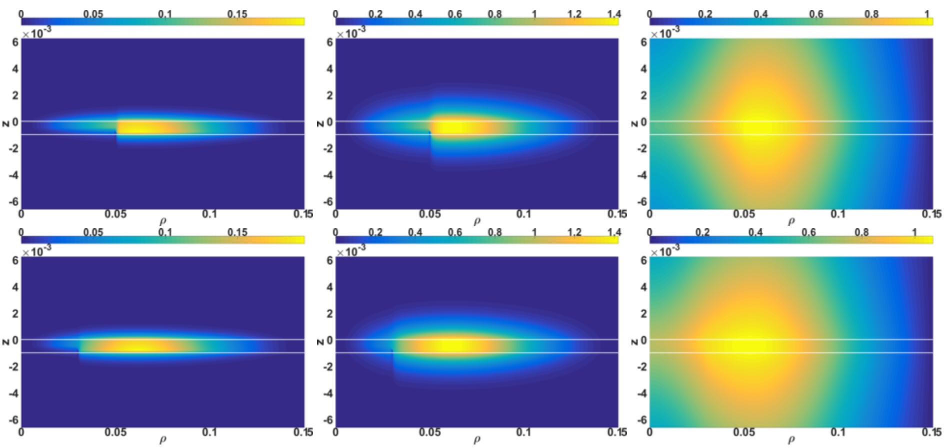

Figure 3. Temperature distribution images in the region of interest for different time and an aluminum plate with defect.
Top: Discontinuity radius: 5 cm. *Bottom:* Discontinuity radius: 3 cm.
Left to the right: Different observation times, $t = t_0$, $t = t_0 + 50$ ms, $t = t_0 + 5$s.

face, when the radius of the corrosion is 5 cm, is plotted compared with the case of the undamaged plate. In Figure 5 the results with a corrosion of radius of 3 cm are given. Since the position of the thermal camera is not fixed, *i.e.* we can have thermal images on both sides of the plate, the difference of temperature is shown in both surfaces.

On both cases, the information about the defect is clear for early times where we are able to distinguish its edges, *i.e.* the size of the defect in the ρ-direction is well defined. When diffusion occurs, the temperature curves of the damaged and undamaged plate are close. In the case of the smaller defect, still we can see that there is a defect in the workpiece but it is impossible to locate its edges. On the other hand, when the defect's

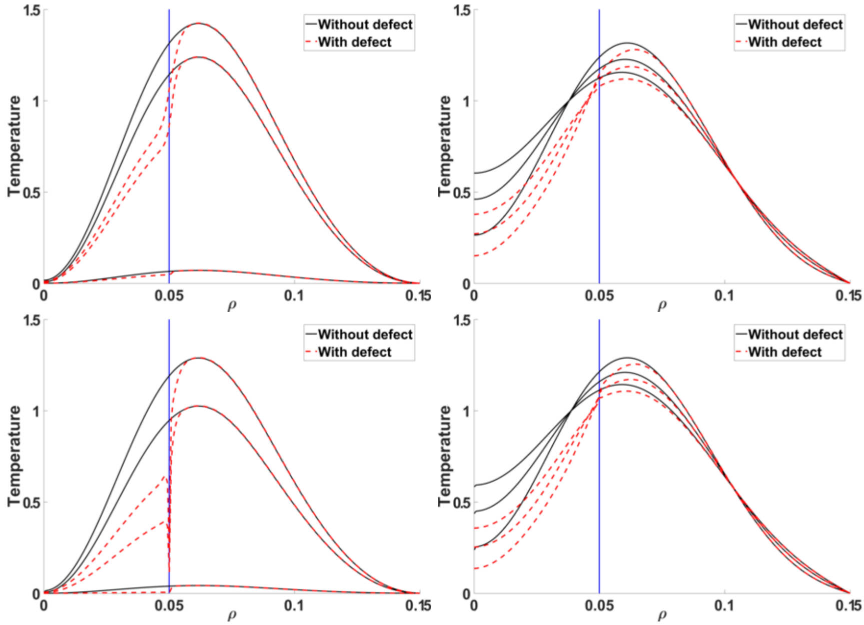

Figure 4. Comparison of the distribution of temperature at the surfaces of the plates with and without defect for different observation times. Defect's radius $r = 5$ cm. *Top:* Upper surface, *Bottom:* Bottom surface. Different observation time: *Left:* 10, 50, 70 ms *Right:* 1, 2, 3s

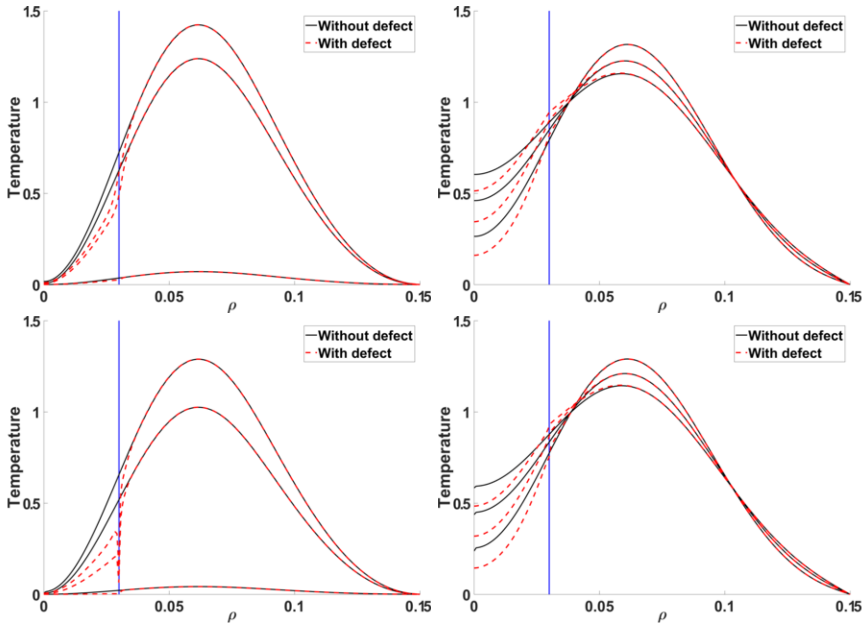

Figure 5. Comparison of the distribution of temperature at the surfaces of the plates with and without defect for different observation times. Defect's radius $r = 3$ cm. *Top:* Upper surface, *Bottom:* Bottom surface Different observation time: *Left:* 10, 50, 70 ms *Right:* 1, 2, 3s

radius is 5 cm, even after 5 seconds the localization of the edges of the defect can be easily achieved through those curves. In general, in ECT we are interested on early times when the difference of the electromagnetic and thermal properties of the workpiece can highlight any presence of a damage on it and this is well shown by the previous results.

4. Conclusions and perspectives

To conclude, a 2D numerical solver based on the finite integration technique has been implemented and used to simulate the behaviour of different materials under inspection by means of eddy current thermography. Both electromagnetic and thermal problems are coupled in a weak way, taking advantage of the large difference between their characteristic time constants. Possible generalizations of this solver are the development of a 3D version or the investigation of strong coupling in the calculation process.

The use of such a numerical solver is important to investigate easily some aspects like effect of piece inhomogeneity or anisotropy, however it can lead to heavy calculations and complicated meshing considerations when addressing 3D configurations. For this reason, this tool will later be used in complement of fast modal methods to adress 3D cases involving canonical geometries like a stratified planar medium.

References

[1] X. Maldague and P. Moore. Infrared and Thermal Testing Nondestructive Testing Handbook, vol. 3. *American Society for Nondestructive Testing*, 2001.
[2] X. Maldague. *Theory and Practice of Infrared Technology for Nondestructive Testing*. Wiley, 2001.
[3] X. Maldague. Introduction to ndt by active infrared thermography. *Materials Evaluation*, 60(9):1060–1073, 2002.
[4] U. Polimeno, D. P. Almond, B. Weekes, and E. W. J. Chen. A compact thermosonic inspection system for the inspection of composites. *Composites Part B: Engineering*, 59:67–73, 2014.
[5] C. Xu, N. Zhou, J. Xie, X. Gong, G. Chen, and G. Song. Investigation on eddy current pulsed thermography to detect hidden cracks on corroded metal surface. *NDT & E International*, 84:27–35, 2016.
[6] R. Marklein. The Finite Integration Technique as a general tool to compute acoustic, electromagnetic, elastodynamic and coupled wave fields. *Review of Radio Science*, 1999.
[7] T. Weiland. A discretization model for the solution of Maxwell's equations for six-component fields. *Archiv Elektronik und Uebertragungstechnik*, 31:116–120, 1977.
[8] T. Theodoulidis and E. Kriezis. *Eddy Current Canonical Problems (with Applications to Nondestructive Evaluation)*. Tech Science Press, 2006.
[9] N. J. Siakavellas. The influence of the heating rate and thermal energy on crack detection by eddy current thermography. *Journal of Nondestructive Evaluation*, 35(2), 2016.